Journal of Marine Research, 48, 287–317, 1990

On the generation and propagation of Rossby waves in an ocean with a zonally shoaling mixed layer

by M. S. Darby[1] and A. J. Willmott[1]

ABSTRACT

This paper presents the theory for freely propagating and forced Rossby waves in a continuously stratified ocean where the bouyancy frequency, N, varies with longitude and depth. In this study zonal variations in N occur because the climatological mixed layer depth, h, varies with longitude.

With the assumption that changes in h occur on a length scale which is large compared to a horizontal wavelength the free modes on a β-plane are examined. It is found that realistic mixed layer depth changes can cause amplitude modulations, the largest amplitudes occurring where the mixed layer is shallowest. The requirement that h variations occur slowly is removed by employing a numerical model to study the free modes in a continuously stratified meridional channel. A criterion, based on the ratio of a horizontal length scale associated with the wave packet and the internal Rossby radius, is derived for determining when a free mode may be affected by the zonal variations in the stratification. Using climatological mixed layer depth data at 35N in the Atlantic (taken from Lamb, 1984) the basin modes are numerically determined. The major response is now concentrated where the mixed layer is deepest. This apparent contradiction is explained.

A general theory is presented for calculating the forced basin mode response in terms of the free modes. As an example, a wind stress curl is applied as a body force over the mixed layer for a finite duration. After the forcing is removed the percentage that each basin mode contributes to the total solution is calculated. It is found that the dominant response to wind stress curl forcing can be significantly affected by the presence of a variable depth mixed layer.

The implication of this study for the interaction between baroclinic Rossby waves and mixed layer dynamics is discussed.

1. Introduction

The purpose of this paper is to examine how zonal variations in the depth of the climatological mixed layer influence the propagation of unforced and forced baroclinic Rossby waves. Lamb (1984) presents the mixed layer climatology for the North Atlantic and this shows that the mixed layer depth can vary zonally at 35N from 70 m to 250 m.

It has been noted by Müller *et al.* (1984) and Stevenson (1983) that the depth and temperature of the upper mixed layer can be influenced by a baroclinic Rossby wave

1. Department of Mathematics, University of Exeter, North Park Road, Exeter, England, EX4 4QE.

field. The authors found that if the vertical velocity associated with the Rossby wave field at the base of the mixed layer is directed upward when the mixed layer deepens in the autumn (due to enhanced mechanical stirring supplied by the wind stress) then significant depth and temperature variations of the mixed layer due solely to the presence of the wave field are obtained. However, both these studies use one-dimensional mixed layer models and the Rossby wave is modelled by a prescribed vertical velocity component (e.g. "a pumping mechanism") at the base of the mixed layer. The amplitude and period of the vertical velocity components is chosen to be representative of that in a baroclinic Rossby wave field. Clearly this approach of incorporating the effects of a Rossby wave field in a mixed layer model is "ad hoc." Nevertheless, both studies indicate that a mixed layer can be "driven from below"; having detailed information about the surface forcing components (e.g. wind stress, various components of the heat flux through the sea surface, evaporation/precipitation data) will not be sufficient input for a prognostic mixed layer model. It is desirable to use a two-dimensional mixed layer model for assessing the influence of a wave field in the thermocline on the mixed layer depth, h. Before this can be done it is important to address the fundamental question of whether baroclinic Rossby waves can "see" (i.e. are modified by) the horizontal variations of h.

Only zonal variations in h will be considered in this study. A local analysis of the problem, based on the assumption that changes in h occur slowly, (throughout this manuscript a quantity is referred to as "slowly varying" if the length scale associated with variations in the x-direction is much larger than a typical horizontal Rossby wavelength in the x-direction) provides a framework for a more detailed numerical study in which a continuously stratified ocean in a meridional channel is examined numerically. Variations along the channel are suppressed by assuming harmonic dependence in that direction (i.e. only one Fourier mode is examined). A similar approach is adopted by Anderson and Gill (1975), Anderson and Killworth (1977) and Willmott and Johnson (1979) when examining the spin-up of a stratified ocean on a meridional β-plane channel.

The plan of the paper is as follows. In Section 2 the local analysis is presented. Section 3 develops the theory of free modes, which reduces to a two-dimensional eigenvalue problem. Section 4 describes the method of solution and presents results of the free modes. Section 5 develops the theory for the forced wave response and Section 6 discusses the limitations and possible extensions of the study.

2. Local analysis of the free mode problem

The ocean domain is located on a mid-latitude β-plane. A local Cartesian coordinate system is chosen, with x directed eastward, y northward and z vertically upward from the ocean floor $z = 0$.

For a continuously stratified Boussinesq fluid, the unforced Rossby wave equation

for the hydrostatic pressure $p(x, y, z, t)$ is given by (see Appendix A)

$$\left[\nabla_h^2 p + f^2\left(\frac{p_z}{N^2}\right)_z\right]_t + \beta p_x = 0, \tag{2.1}$$

where ∇_h^2 is the two-dimensional Laplacian operator, f is the constant Coriolis parameter evaluated at the latitude of the β-plane origin, β is the north-south gradient of f and N is the Brunt-Väisälä frequency (or buoyancy frequency).

In this study zonal variations of the mixed layer depth will be modelled by suitable distributions for $N = N(x, z)$. A similar approach is adopted in a study of internal wave propagation in a randomly stratified fluid by Mysak and Howe (1976) where they prescribe $N(x, z)$. Mysak (1978) also reviews the literature on internal wave propagation through an ocean in which N has prescribed horizontal variation. In these studies the precise mechanism that maintains the prescribed N distribution is not considered. This approach will be adopted here.

At middle latitudes the large-scale mean flow contributes to the maintenance of the climatological $N(x, y, z)$. On a β-plane the existence of nonzonal mean flows implies that an external forcing field is acting (typically the wind stress curl). Hence $N(x, z)$ cannot support an unforced geostrophically balanced meridional velocity field. From the point of view of this study, an external forcing (unspecified) can be considered to maintain the specified $N(x, z)$. The influence of mean flows on baroclinic Rossby waves is considered by Killworth (1979), who shows that meridional flows are less effective than zonal flows at altering Rossby wave propagation. Indeed, Killworth (1979) finds that barotropic meridional flows of the order of 30 cm s^{-1} are required before Rossby wave reflection occurs. The climatological distributions of $N(x, z)$ considered here cannot support geostrophic flows of this magnitude normal to the $x - z$ plane. At worst, meridional flows will deflect, rather than prohibit, wave propagation. However, to analyze Rossby wave propagation in an ocean in which $N = N(y, z)$ will require a treatment of the zonal geostrophically balanced mean flow supported by the stratification.

It is convenient to nondimensionalize (2.1) using the following dimensionless variables, denoted by circumflexes:

$$(\hat{x}, \hat{y}) = L^{-1}(x, y), \qquad \hat{z} = H^{-1}z, \qquad \hat{t} = ft, \qquad \hat{N} = f^{-1}N,$$
$$\hat{p} = p/(\rho_* L^2 f^2), \qquad \hat{\beta} = \beta L f^{-1}$$

where ρ_* is a constant reference density, L is any suitable length scale and H is the depth of the ocean. On dropping the circumflexes the dimensionless form of (2.1) becomes

$$\left[\nabla_h^2 p + \sigma^2\left(\frac{p_z}{N^2}\right)_z\right]_t + \beta p_x = 0, \tag{2.2}$$

where $\sigma = L/H$ is the aspect ratio.

If N is a function of z alone then (2.2) can be separated into the vertical and horizontal problems:

$$\left(\frac{\Pi_{nz}}{N^2}\right)_z + \frac{\Pi_n}{h_n} = 0 \tag{2.3a}$$

and

$$\left[\nabla_h^2 \check{p}_n - \frac{\sigma^2}{h_n}\check{p}_{nz}\right]_t + \beta \check{p}_{nx} = 0, \tag{2.3b}$$

where $p(x, y, z, t) = \Pi_n(z)\check{p}_n(x, y, t)$ and h_n is a separation constant. The suffix n has been introduced to emphasise that h_n is associated with a particular mode. If we assume that changes in mixed layer depth, h, occur on a large length scale (relative to a horizontal wavelength in the x direction) then solutions of (2.3) are locally valid, but now $h_n = h_n(x)$ is a slowly varying function of x. Subject to suitable boundary conditions and a specified $N(x, z)$, solution of (2.3a) gives $h_n(x)$ which in turn is used in the solution of (2.3b) for $\check{p}$.

a. Vertical problem. A realistic profile of N^2 is,

$$N^2 = \begin{cases} 0, & z_m(x) \le z \le 1 \\ N_0^2 e^{\alpha(z - z_m)}, & 0 \le z \le z_m. \end{cases} \tag{2.4}$$

where α and N_0 are chosen to give a realistic buoyancy frequency and $\delta = (1 - z_m) = h/H$ is the depth of the mixed layer. Zero vertical velocity at $z = 0, 1$ is specified by (see Ch. 3, LeBlond and Mysak, 1978)

$$\Pi_{nz} = 0 \qquad \text{at } z = 0, 1. \tag{2.5}$$

The problem specified by (2.3a), (2.4) and (2.5) has been solved by Bryan and Ripa (1978). Here we are only interested in the variation of h_n with δ. Defining the quantities,

$$\chi_n^2 = \frac{4N_0^2 e^{\alpha\delta}}{\alpha^2 h_n}, \qquad s^* = \exp\left(-\frac{\alpha\delta}{2}\right), \qquad \epsilon = \exp\left(-\frac{\alpha}{2}\right),$$

it is found that the eigenvalue χ_n satifies the equation

$$\mathcal{C}_0(\chi_n s^*) = \tfrac{1}{2}\alpha\delta\chi_n s^* \mathcal{C}_1(\chi_n s^*), \tag{2.6}$$

where

$$\mathcal{C}_i(\zeta) = J_i(\zeta) + d_n Y_i(\zeta)$$

and

$$d_n = -J_0(\chi_n \epsilon)/Y_0(\chi_n \epsilon).$$

In (2.6) J_n and Y_n denote the n$^{\text{th}}$-order Bessel functions of the first and second kind respectively.

b. Horizontal problem. To solve (2.3b) we make use of a direct asymptotic expansion and assume a solution exists of the form (Whitham, 1974),

$$\check{p}(x, y, t) = e^{i\theta(x,y,t)} \sum_{n=0}^{\infty} A_n(x) \tag{2.7}$$

where it is understood that θ_x, θ_y, θ_t and A_0 are order one quantities and differentiation with respect to x increases the order by one as does raising the subscript of A_n. Substitution of (2.7) into (2.3b) and equating first order terms to zero gives,

$$(k - \gamma)^2 + l^2 = \gamma^2 - \frac{\sigma^2}{h_n}, \tag{2.8}$$

where $k = \theta_x$, $l = \theta_y$, $\omega = -\theta_t$ and $\gamma = -\beta/2\omega$. The next order gives the required relation between variations in k and A_0, namely,

$$\frac{dA_0}{dx} = \frac{A_0}{2(\gamma - k)} \frac{dk}{dx},$$

which can be integrated to give

$$A_0 = \frac{C}{|\gamma - k|^{1/2}}, \tag{2.9}$$

where C is an arbitrary constant. The interpretation of (2.9) is clear when it is remembered that (2.8) is actually a first-order nonlinear partial differential equation for $\theta(x, y, t)$ which can be solved by integrating along the characteristics defined by

$$\left.\begin{aligned} \frac{dx}{ds} &= -(k - \gamma), \quad \frac{dy}{ds} = -l, \quad \frac{dk}{ds} = \frac{\sigma^2}{2}\left(\frac{1}{h_n}\right)_x, \\ \frac{dl}{ds} &= \frac{\sigma^2}{2}\left(\frac{1}{h_n}\right)_y, \quad \frac{dt}{ds} = \frac{k\gamma}{\omega}, \end{aligned}\right\} \tag{2.10}$$

where s measures distance along a characteristic (time increases as s increases). Since h is a function of x only, l and ω are conserved along a characteristic. The group velocity vector is always tangential to the rays defined by (2.10). Therefore it is clear from (2.9) and (2.10) that large values of A_0 can be expected where $(k - \gamma)$ is small, i.e. in regions where the direction of energy propagation is most closely aligned to the meridional direction.

Table 1. Eigenvalues, χ_n, and amplitudes, A_0, for $\alpha^{-1} = 254.51$ m and various values of mixed layer depth, h, and ocean depth, H.

h(m)	H(m)	χ_n	A_0	$\lvert k - \gamma \rvert$m^{-1}
50	3000	2.70882	100	3.14×10^{-6}
100	3000	2.73823	45.9	1.49×10^{-5}
150	3000	2.79927	40.1	1.95×10^{-5}
200	3000	2.89182	37.5	2.23×10^{-5}
250	3000	3.01423	36.0	2.43×10^{-5}
50	4000	2.62644	57.6	9.46×10^{-6}

As an example, we determine how A_0 may vary as a wave propagates from a region where the mixed layer depth is 50 m to one where it is 250 m. For various values of h and H, Table 1 shows χ_n and A_0. The dimensional parameter values (see Willmott and Mysak, 1980) $N_0 = 0.011045$ s^{-1}, $\alpha^{-1} = 254.51$ m and $f = 1.2 \times 10^{-4}$ s^{-1} were chosen to be typical of the northeast Pacific at 55N. In order to compute the variations of $\lvert k - \gamma \rvert$ with $h(x)$ a reference value must be specified. Since we find that $\lvert k - \gamma \rvert$ is smallest where h is smallest we choose, for illustration, the arbitrary value $\lvert k - \gamma \rvert_{\min} = \pi/10^6$ m^{-1} where $h = 50$ m (a smaller value would cause A_0 to be more sensitive to changes in $h(x)$ where h is small). In order to compute Table 1 we did not need to specify l. However, the results only apply to a realistic ocean if $l \leq \lvert k - \gamma \rvert_{\max}$ so that the ray will reach regions of small h before travelling an unreasonable distance in the meridional direction. Since $\lvert k - \gamma \rvert_{\max} = 2.43 \times 10^{-5}$ m^{-1} (corresponding to a wavelength of 258 km) this is not an unreasonable restriction on l. It is interesting to note that a 200 m change in mixed layer depth causes more change in A_0 then a 1000 m change in ocean depth. Furthermore, the largest value of A_0 occurs where h is smallest.

Table 2 contains the analogous results to Table 1 except $\alpha^{-1} = 650$ m. For this case the mixed layer depth changes have a smaller effect on the amplitude, whereas the topographic change of 1000 m has almost the same effect as when $\alpha^{-1} = 254.51$ m. This emphasizes that it is the rapid exponential fall off in Brunt-Väisälä frequency below the mixed layer which allows realistic mixed layer depth changes to cause large amplitude changes.

Table 2. Analogous results to Table 1 except $\alpha^{-1} = 650.0$ m.

h(m)	H(m)	χ_n	A_0	$\lvert k - \gamma \rvert$m^{-1}
50	3000	3.31221	100	3.14×10^{-6}
100	3000	3.31693	73.2	5.86×10^{-6}
150	3000	3.32837	64.8	7.48×10^{-6}
200	3000	3.34809	60.3	8.64×10^{-6}
250	3000	3.37684	57.4	9.53×10^{-6}
50	4000	3.04398	62.9	7.95×10^{-6}

It is important to emphasize that for the case $h = h(x, y)$ both k and l may vary along a ray. The amplitude equation becomes

$$\frac{1}{A_0}\frac{\partial A_0}{\partial x} + \frac{1}{A_0}\frac{\partial A_0}{\partial y}\left(\frac{l}{k-\gamma}\right) = \left[\frac{1}{2(\gamma - k)}\right]\left(\frac{\partial k}{\partial x} + \frac{\partial l}{\partial y}\right).$$

This must in general be solved numerically but there is now no reason to expect A_0 to have it's maximum value where h is smallest.

In summary, we expect that realistic changes in mixed layer depth may have a profound effect on Rossby waves, in this particular case, causing the modulating amplitude envelope of a wave packet to concentrate energy where the mixed layer depth is smallest. This has important implications for the inclusion of Rossby wave fields into a mixed layer model. However, it is important to note that we do not claim this analysis to be an exhaustive study of the problem but rather an attempt to isolate, in the simplest possible manner, what effect mixed layer depth variations may have on Rossby waves. Although an extension of this section to include more general variations in mixed layer depth (i.e. meridional variations) is possible we feel that a numerical model is more valuable. Such a model is not restricted to slow (and from an oceanographic point of view somewhat unrealistic) variations in h and can be used to study the forced response.

3. Formulation of the problem for free-modes in a meridional channel

In this section the theory of free basin modes in a continuously stratified meridional channel of width L and depth H is developed. With respect to the (dimensionless) coordinate system the channel walls are at $x = 0, 1$.

Assume harmonic dependence in y so that

$$p = \tilde{p}(x, z, t)\cos(ly),$$

where it is understood that p is a real function and l is a constant dimensionless wavenumber. Then (2.2) becomes

$$\left[\tilde{p}_{xx} - l^2\tilde{p} + \sigma^2\left(\frac{\tilde{p}_z}{N^2}\right)_z\right]_t + \beta\tilde{p}_x = 0. \tag{3.1}$$

Seek a solution of (3.1) of the form

$$\tilde{p}(x, z, t) = a\phi\exp[i(\gamma x - \omega t)] + a^*\phi\exp[-i(\gamma x - \omega t)], \qquad \omega > 0, \tag{3.2}$$

where $\phi = \phi(x, z)$, $\gamma = -\beta/2\omega$, a is a constant complex coefficient and the asterix is used to denote the complex conjugate. By seeking a solution of the form (3.2) it ensures

that p will be real. Substituting (3.2) into (3.1) gives

$$\phi_{xx} + \lambda\phi + \sigma^2\left(\frac{\phi_z}{N^2}\right)_z = 0, \tag{3.3a}$$

where

$$\lambda = \gamma^2 - l^2.$$

Boundary conditions for (3.3a) are obtained from demanding no normal flow through rigid boundaries and zero vertical velocity at the mean sea surface $z = 1$. In terms of ϕ (see Ch. 3, LeBlond and Mysak, 1978) this requires

$$\left.\begin{aligned} \phi &= 0, \quad \text{at } x = 0, 1 \\ \phi_z &= 0, \quad \text{at } z = 0, 1. \end{aligned}\right\} \tag{3.3b}$$

System (3.3) defines a 2-dimensional eigenvalue problem for eigenvalue λ and eigenfunction ϕ. Once the eigenvalues are obtained the frequency ω is determined from

$$\omega = \tfrac{1}{2}\beta(\lambda + l^2)^{-1/2},$$

where l is specified of course.

At this stage it is convenient to derive the orthogonality condition satisfied by the free modes. In Section 5 it will be used to solve the forced wave problem. Let

$$\left.\begin{aligned} r_n &= b_n\phi_n \exp\left[i(\gamma_n x - \omega_n t)\right] \\ r_n^* &= b_n\phi_n \exp\left[-i(\gamma_n x - \omega_n t)\right] \end{aligned}\right\} \tag{3.4}$$

where b_n are normalizing coefficients, ω_n is the wave frequency associated with eigenvalue λ_n and $\phi_n(x, z)$ is the corresponding non-separable eigenfunction. It is straightforward (the details, including the value of b_n, are presented in Appendix B) to show that the normalized orthogonality conditions that (3.4) satisfy are

$$\int_D\int r_m r_{nx}^* \, dx \, dz = i\delta_{mn} \tag{3.5a}$$

and

$$\int_D\int r_m r_n^* \, dx \, dz = \frac{\delta_{mn}}{|\gamma_m|}, \tag{3.5b}$$

where δ_{mn} is the Kronecker delta and D is the rectangular cross-sectional area of the basin in the $x - z$ plane.

4. Numerical determination of the eigenvalues and eigenfunctions

The significant nonzero form of N is contained within the upper 1 km of the ocean (see Emery *et al.*, 1984). Below 1 km the value of N is close to zero. This presents a

problem if (3.3) is to be solved numerically using a regularly spaced vertical grid because a large number of grid points are required to adequately resolve the upper ocean stratification.

By introducing a stretched vertical coordinate, the number of vertical grid points required to resolve N can be dramatically reduced. Define the stretched coordinate

$$\eta = \frac{z(1-b)}{z-b}, \qquad b > 1. \tag{4.1}$$

Then $0 \le \eta \le 1$ because $0 \le z \le 1$. Points which are regularly spaced along the η-axis will be irregularly spaced when mapped to the z-axis using (4.1). Furthermore, the grid along the z-axis has small step size near the ocean surface ($z = 1$) and progressively larger step size towards the ocean floor ($z = 0$). The degree of stretching is governed by the value of b. A regularly spaced grid in $x - \eta$ space is mapped onto a stretched grid in $x - z$ space on which (3.3) is solved. The details, including the numerical methods used to solve the problem, are presented in Appendix C.

Within the mixed layer N is almost zero because the density is well mixed in the vertical. To model the climatological $N(x, z)$ the distribution

$$N^2(x, z) = \begin{cases} 10^{-3}N_0^2, & z_m(x) \le z \le 1 \\ N_0^2 \exp\left[\alpha(z - z_m)\right], & 0 \le z \le z_m, \end{cases}$$

is specified. The values of α and N_0 are chosen to give a buoyancy frequency profile typical of that in the North Atlantic.

The free modes are calculated for:

(a) mixed layer with zonal depth variation. The depth variation is taken from the climatology of Lamb (1984) at 35N in the Atlantic.

(b) a constant mixed layer depth, taken to be the average value from (a).

In both cases the channel is 7000 km wide, 3 km deep, $f = 8.35 \times 10^{-5}\ \mathrm{s}^{-1}$ and $\beta = 1.87 \times 10^{-11}\ \mathrm{m}^{-1}\mathrm{s}^{-1}$. The regular grid in $x - \eta$ space has dimension 20×40 and the stretching parameter $b = 1.2$. With this value of b there are only 6 points below 1500 m and the resolution of the upper ocean N is high enough to accurately resolve the 6$^{\text{th}}$ vertical baroclinic mode. The dimensionless stratification parameters are $N_0^{-2} = 7.83 \times 10^{-5}$, $\alpha = 4.61$ (see Emery *et al.*, 1984).

When N is independent of x, the free modes satisfying (3.3) are separable in x and z. Indeed, when $N = N_0$ (constant) throughout the domain the eigenfunctions of (3.3a) are

$$\phi_{m,n} = \sin(m\pi x)\cos(n\pi z), \tag{4.2a}$$

with associated eigenvalues

$$\lambda_{m,n} = m^2\pi^2 + \left(\frac{\sigma}{N_0}\right)^2 n^2\pi^2 \tag{4.2b}$$

where $m = 1, 2, 3, \ldots$ and $n = 0, 1, 2, \ldots$. Choosing σ and N_0 to be typical of the Atlantic at 35N (and m reasonably small) leads to eigenvalues which occur in well separated clusters corresponding to the value of the index n. The case $n = 0$ corresponds to the barotropic mode; $n \geq 1$ corresponds to the n^{th} baroclinic mode. Within an eigenvalue cluster the values are relatively close, different eigenvalues corresponding to different horizontal structure (i.e. varying m).

The gross features of this solution are still displayed when (3.3) is solved for $N = N(x, z)$. This means that it is still possible to classify an eigenfunction according to the number of zero crossings in the vertical (i.e. the barotropic mode has no zero crossings; the first baroclinic mode has one zero crossing and so on). However, the eigenfunctions are, of course, no longer separable.

When referring to the eigenvalues and eigenfunctions associated with $N(x, z)$ the following terminology will be used. Let $\lambda_{i,j}$ represent the eigenvalue corresponding to an eigenfunction $\phi_{i,j}$ which has i half wavelengths in the x-direction and j half wavelengths in the z-direction (e.g. $\lambda_{2,3}$ is the eigenvalue corresponding to eigenfunction $\phi_{2,3}$ which is the third baroclinic mode with a complete wavelength across the channel).

For the stratification (a), Figure 1(a) shows contours of $\phi_{1,1}$ and Figure 1(b) displays a plot of the associated pressure field at a depth of 400 m below the sea surface. The wavenumber l is chosen to give a meridional wavelength of 500 km. Figure 2 displays the analogous plots for the eigenfunction $\phi_{3,1}$ and the associated pressure field. All contours of ϕ are presented in $x - \eta$ space for clarity. The eigenfunctions are normalized so that $|\phi| \leq 1.0$.

It is clear that a horizontally varying mixed layer depth has a significant effect on the free Rossby wave modes when Figures 1 and 2 are compared with Figures 3 and 4. Figures 3 and 4 are the analogous solutions shown in Figures 1 and 2 respectively, for stratification (b). An important feature in Figures 1 and 2 is that the maximum wave response is concentrated in the region where the mixed layer is deepest. The apparent contradiction with the results of Section 2 (where the local analysis led to maximum wave response where the mixed layer is shallowest) is explained at the end of this section.

A natural question to ask is when do the free modes "see" the horizontal variations in stratification. Variations in horizontal stratification will be significant when

$$\left|\frac{\sigma^2}{\phi_{xx}}\left(\frac{\phi_z}{N^2}\right)_z\right| \equiv S \gg 1, \tag{4.3}$$

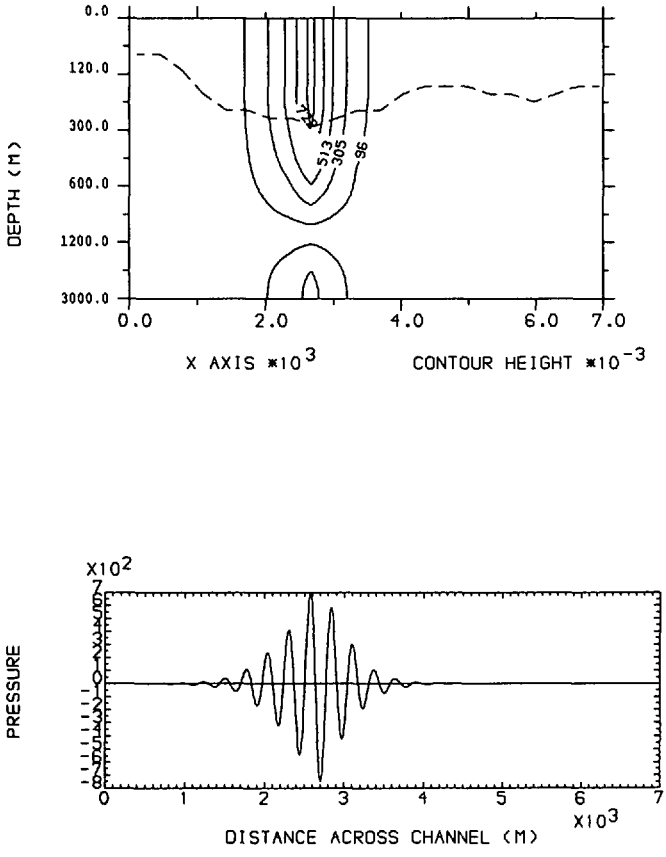

Figure 1. (a) Contours of $\phi_{1,1}(x, z)$ for stratification (a) with $L = 7000$ km and $H = 3$ km. The dashed line indicates the position of the mixed layer base. (b) Plot of pressure, $p_{1,1}(x)$, at a depth of 400 m for stratification (a) with $L = 7000$ km and $H = 3$ km.

upon examining (3.3a). Even the most distorted eigenfunctions (see Fig. 1(a)) still exhibit the gross features of the separable solution (4.2). Hence

$$S \approx \frac{\sigma^2 n^2}{\overline{N}^2 m^2},$$

where $\overline{N}$ is a typical value of the dimensionless buoyancy frequency and m, n are integers defined in (4.2). Clearly the barotropic mode ($n = 0$) is unaffected by stratification. Define the quantities

$$\nu_m = \frac{2L}{m} \quad \text{and} \quad r_{in} = \frac{\overline{N}_d H}{nf},$$

where ν_m is an estimate of the dimensional wavelength of $\phi_{m,n}$, $\overline{N}_d = f\overline{N}$ and r_{in} is the n^{th}

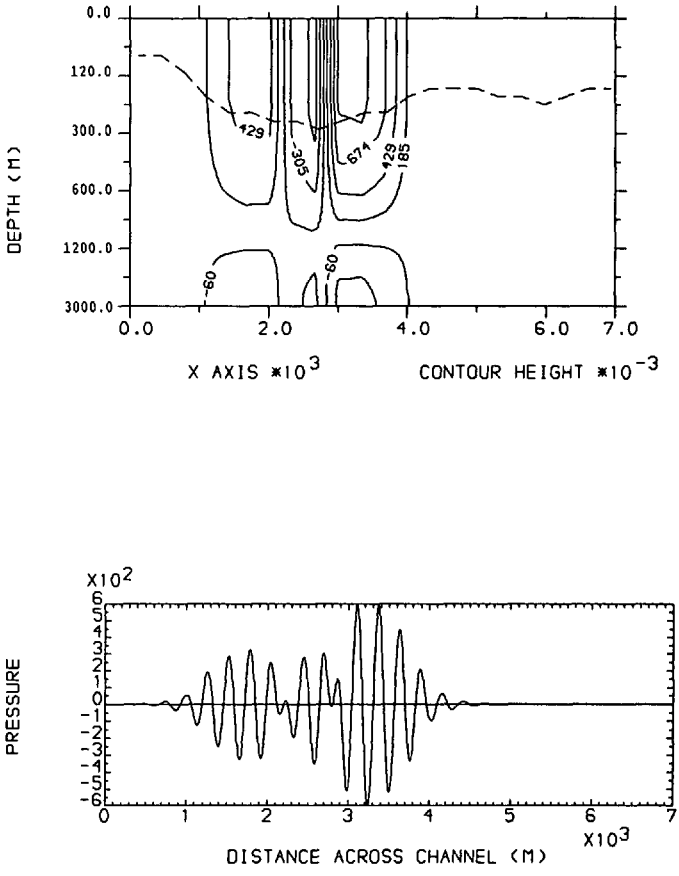

Figure 2. (a) Contours of $\phi_{3,1}(x, z)$ for stratification (a) with $L = 7000$ km and $H = 3$ km. The dashed line indicates the position of the mixed layer base. (b) Plot of pressure, $p_{3,1}(x)$, at a depth of 400 m for stratification (a) with $L = 7000$ km and $H = 3$ km.

internal Rossby radius. Then S can be rewritten as

$$S \approx \left(\frac{\nu_m}{2r_{in}}\right)^2.$$

Therefore an eigenfunction $\phi_{m,n}$ can be expected to be affected by horizontal variations in stratification if the horizontal wavelength associated with $\phi_{m,n}$ is much larger than the n^{th} internal Rossby radius. For the results shown in Figures 1 and 2, $\sigma^2 = 5.4 \times 10^6$ and $\overline{N}^{-2} = 3.9 \times 10^{-4}$ (this value of $\overline{N}$ gives a good estimate of the numerically determined eigenvalues λ for the stratification (a)) in which case

$$S \approx 2131.5\left(\frac{n}{m}\right)^2.$$

When $n = 1$ (a first baroclinic mode-type eigenfunction) (4.3) suggests that horizontal

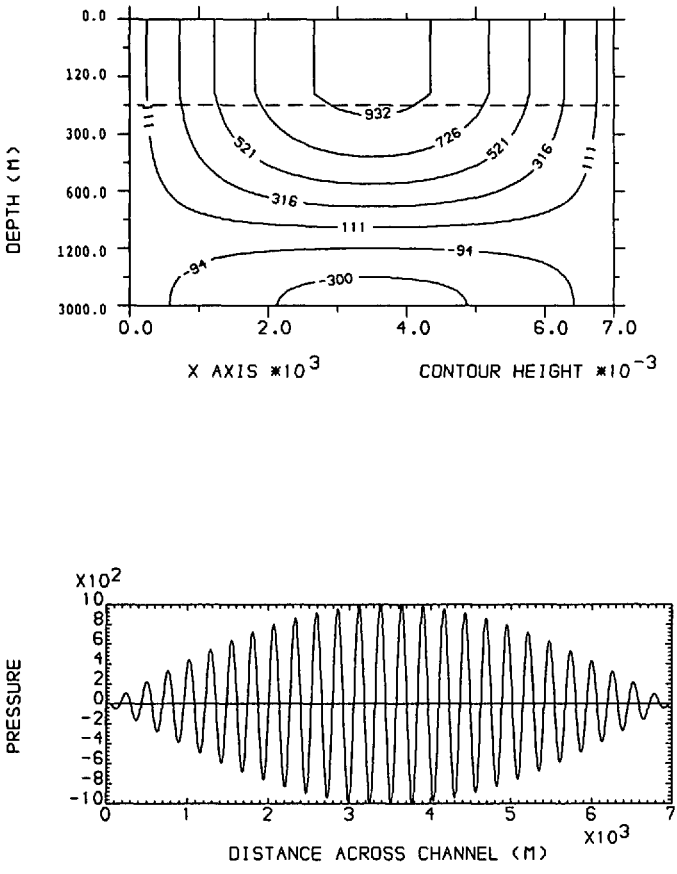

Figure 3. (a) Contours of $\phi_{1,1}(x, z)$ for stratification (b) with $L = 7000$ km and $H = 3$ km. The dashed line indicates the position of the mixed layer base. (b) Plot of pressure, $p_{1,1}(x)$, at a depth of 400 m for stratification (b) with $L = 7000$ km and $H = 3$ km.

variations of the mixed layer depth will be important provided $m \leq 14$ (i.e. $S \geq 10$). In Figures 1(a) and 2(a) the eigenfunctions are severely distorted by the horizontal stratification variations, as predicted by (4.3). To reinforce this point, (4.3) is satisfied when $m = 6$ and Figure 5(a) displays contours of $\phi_{6,1}$ while Figure 5(b) shows a plot of pressure at 400 m below the surface as a function of x. Figure 6 shows the equivalent plots of Figure 5, but with stratification (b).

Now consider a case when horizontal variations of N are unimportant for the eigenfunction behavior. Choose a narrow channel with $L = 1000$ km and $H = 4$ km. A regularly spaced grid in $x - \eta$ space of 31×21 is used with increased stretching ($b = 1.1$) in the z-direction to compensate for fewer points in that direction. Then employing the stratification of the previous experiments,

$$S \approx 24.5 \left(\frac{n}{m}\right)^2.$$

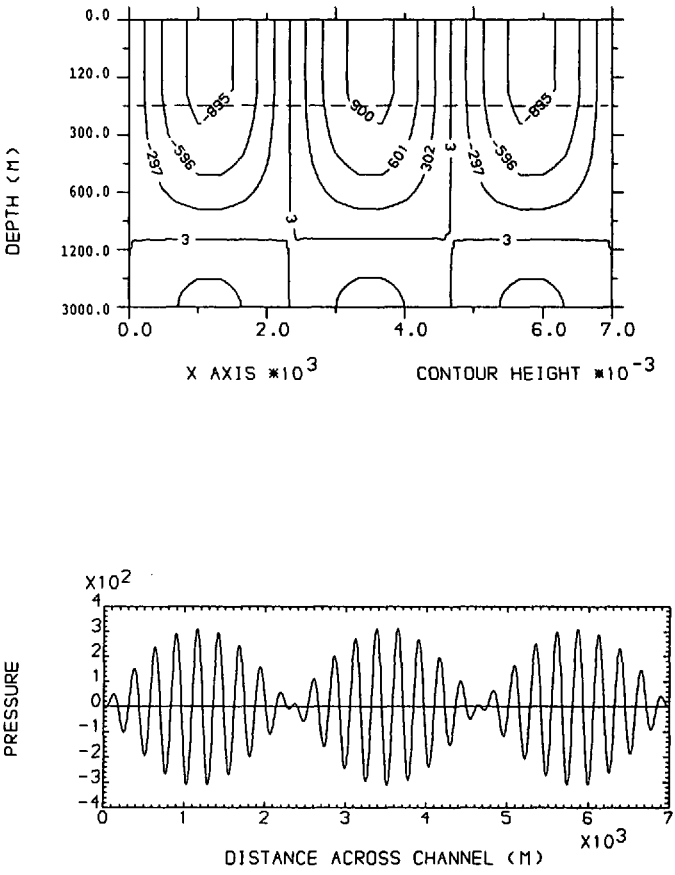

Figure 4. (a) Contours of $\phi_{3,1}(x, z)$ for stratification (b) with $L = 7000$ km and $H = 3$ km. The dashed line indicates the position of the mixed layer base. (b) Plot of pressure, $p_{3,1}(x)$, at a depth of 400 m for stratification (b) with $L = 7000$ km and $H = 3$ km.

Consider a first baroclinic mode-type eigenfunction ($n = 1$). Figure 7(a) shows contours of $\phi_{3,1}$ and Figure 7(b) displays the pressure at a depth of 300 m for the stratification (a). In this case $N(x, z)$ produces little distortion of the eigenfunctions, and this agrees with the value of $S \approx 2.7$ (i.e. violating (4.3)). Figure 8 shows the equivalent plots of Figure 7, with stratification (b).

To understand the results of this Section in the light of the ray theory presented in Section 2 we write

$$\phi(x, z) = A(x) \sin (k_\phi x)$$

where k_ϕ is the local horizontal wavenumber associated with $\phi(x, z)$ and $A(x)$ is the slowly varying amplitude. Then using (3.2)

$$\tilde{p}(x, z, t) = 2A \sin (k_\phi x) \cos (\gamma x - \omega t) \tag{4.4}$$

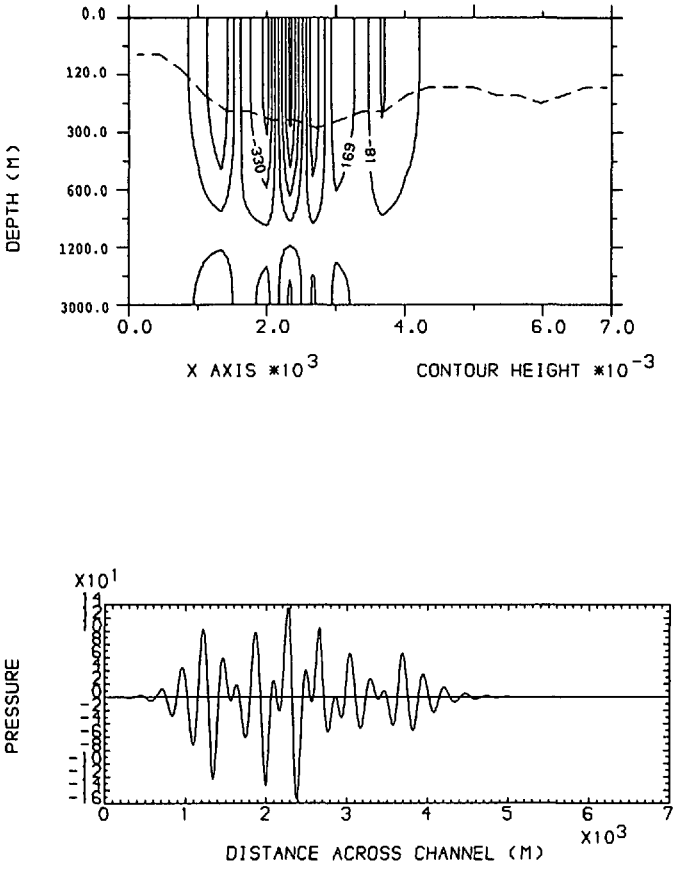

Figure 5. (a) Contours of $\phi_{6,1}(x, z)$ for stratification (a) with $L = 7000$ km and $H = 3$ km. The dashed line indicates the position of the mixed layer base. (b) Plot of pressure, $p_{6,1}(x)$, at a depth of 400 m for stratification (a) with $L = 7000$ km and $H = 3$ km.

where, without loss of generality we have assumed that $a = 1$ and $k_\phi > 0$. Rewriting (4.4) in the form

$$\tilde{p} = A\{\sin[(\gamma + k_\phi)x - \omega t] - \sin[(\gamma - k_\phi)x - \omega t]\} \tag{4.5}$$

shows that there are two waves present with horizontal wavenumbers in the x-direction given by $k_1 \equiv \gamma + k_\phi$ and $k_2 \equiv \gamma - k_\phi$. Notice that $|\gamma - k_1| = |\gamma - k_2| = k_\phi$. Using (2.9) to estimate A, we find that (4.4) can be written as

$$\tilde{p} = \frac{2}{|k_\phi|^{1/2}} \sin(k_\phi x) \cos(\gamma x - \omega t).$$

Thus

$$\lim_{k_\phi \to 0} \tilde{p} \approx 2k_\phi^{1/2} x \cos(\gamma x - \omega t). \tag{4.6}$$

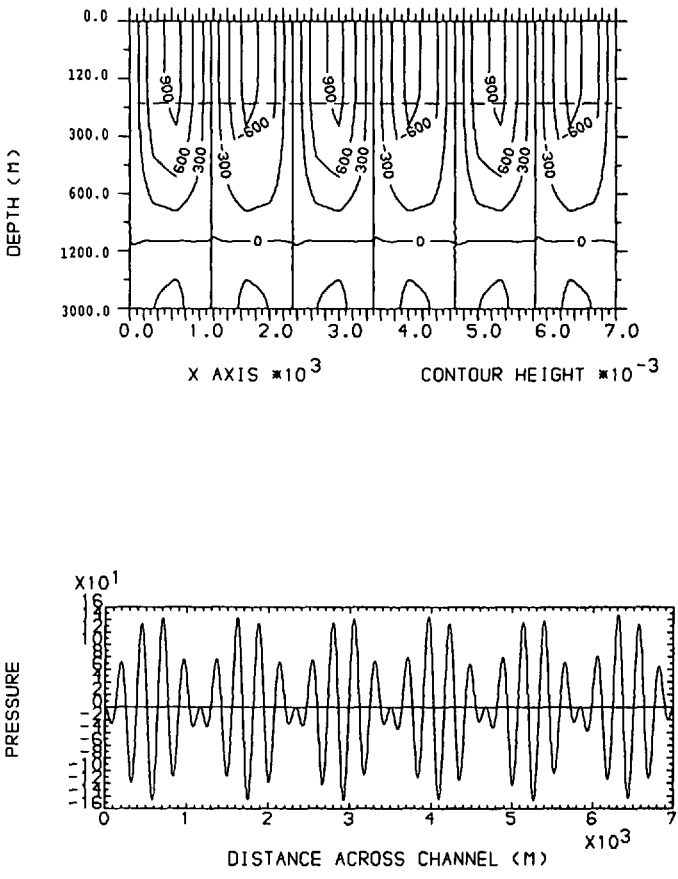

Figure 6. (a) Contours of $\phi_{6,1}(x, z)$ for stratification (b) with $L = 7000$ km and $H = 3$ km. The dashed line indicates the position of the mixed layer base. (b) Plot of pressure, $p_{6,1}(x)$, at a depth of 400 m for stratification (b) with $L = 7000$ km and $H = 3$ km.

We now estimate whether the size of the change in k_ϕ found numerically in this section is consistent with the analytical results of Section 2. Of course the analytical theory of Section 2 assumes h variations occur slowly but we still hope there will be order of magnitude agreement. The results shown in Table 2 (described in Section 2) use parameter values similar to those used to calculate Figures 1, 2 and 5 so using Table 2 we expect the change in $|k - \gamma|$ (call this $\Delta|k - \gamma|$) to be approximately 6.4×10^{-6} m^{-1}. Even the most distorted eigenfunctions exhibit the gross features of the idealized solution (4.2a) so we estimate the average (across the channel) value of $k_\phi(x)$ to be

$$\overline{k}_\phi = \frac{m\pi}{L} = \frac{m\pi}{7 \times 10^6}\ \mathrm{m}^{-1}.$$

If $\Delta|k - \gamma| > \overline{k}_\phi$ the local analysis of Section 2 implies k_ϕ will be very small where the

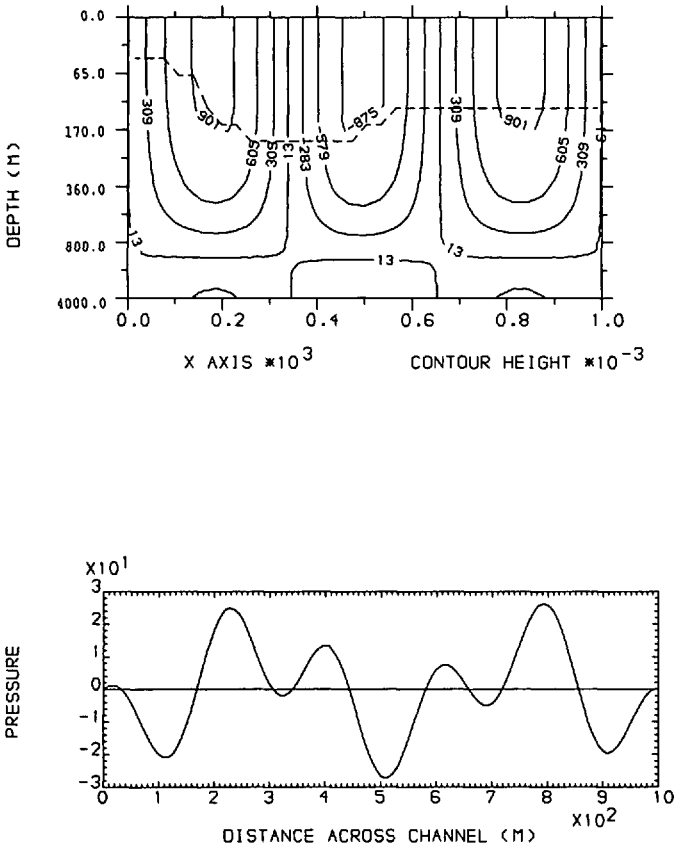

Figure 7. (a) Contours of $\phi_{3,1}(x, z)$ for stratification (a) with $L = 1000$ km and $H = 3$ km. The dashed line indicates the position of the mixed layer base. (b) Plot of pressure, $p_{3,1}(x)$, at a depth of 400 m for stratification (a) with $L = 1000$ km and $H = 3$ km.

mixed layer is shallow. For this case $\Delta|k - \gamma| > \overline{k}_\phi$ for $m \leq 14$ (incidentally in good agreement with the condition $S \gg 1$) and since $m \leq 6$ for Figures 1, 2 and 5 we expect $k_\phi \longmapsto 0$ in the region where h is small. This explains why the distorted basin modes, discussed in this section, have maximum response where k_ϕ is maximum and the mixed layer is deepest. Where the mixed layer is shallow k_ϕ and hence $\tilde{p}$ (see (4.6)) are both small.

5. Forced response

When an external forcing field acts for a finite time and is subsequently removed, the resulting solution will be made up from an infinite sum of the free modes. The question of interest is what fraction of the total solution does a particular eigenfunction contribute? The orthogonality properties of the free modes derived in Section 3 allows this question to be answered.

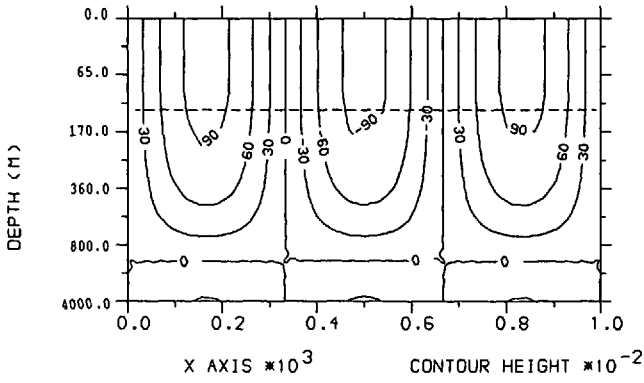

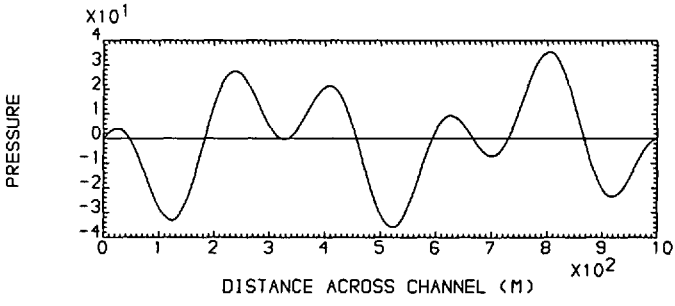

Figure 8. (a) Contours of $\phi_{3,1}(x, z)$ for stratification (b) with $L = 1000$ km and $H = 3$ km. The dashed line indicates the position of the mixed layer base. (b) Plot of pressure, $p_{3,1}(x)$, at a depth of 400 m for stratification (b) with $L = 1000$ km and $H = 3$ km.

The pressure associated with the forced wave response satisfies

$$\left[\nabla_h^2 p + \sigma^2 \left(\frac{p_z}{N^2}\right)_z\right]_t + \beta p_x = \hat{g},$$

where $\hat{g}(x, y, z, t) = g(x, y, z, t)/\rho_* f^3$ is a prescribed dimensionless external forcing field. In this study g will correspond to the wind stress curl acting as a body force in the mixed layer. Dropping the circumflex, let $g(x, y, z, t) = \tilde{g}(x, z, t) \cos(ly)$. Then the analogue of (3.1) is

$$\left[\tilde{p}_{xx} - l^2 \tilde{p} + \sigma^2 \left(\frac{p_z}{N^2}\right)_z\right]_t + \beta \tilde{p}_x = \tilde{g}. \tag{5.1}$$

Write

$$\tilde{p}(x, z, t) = \sum_{n=1}^{\infty} (a_n r_n + a_n^* r_n^*), \tag{5.2a}$$

$$\tilde{g}(x, z, t) = \sum_{n=1}^{\infty} (g_n r_n + g_n^* r_n^*), \tag{5.2b}$$

where r_n, r_n^* are normalized eigenfunctions (i.e. satisfying (3.5)), a_n and g_n are complex functions of time only. Substitute (5.2) into (5.1) and employ (B1), (B2) to obtain

$$\frac{i\beta}{\omega_n}\left[\sum_{n=1}^{\infty} (-a_{nt} r_{nx} + a_{nt}^* r_{nx}^*)\right] = \sum_{n=1}^{\infty} (g_n r_n + g_n^* r_n^*). \tag{5.3}$$

Multiply each side of (5.3) by r_m^*, integrate over the domain D and employ (3.5) to give

$$\frac{da_n}{dt} = -\frac{\omega_n}{|\gamma_n|\beta} g_n. \tag{5.4}$$

For a specified $\tilde{g}$, the coefficients g_n are readily determined and (5.4) can be solved subject to a suitable boundary condition. To determine g_n multiply each side of (5.2b) by r_m^*, integrate over the region D and employ (3.5). The result is that

$$g_n(t) = |\gamma_n| \int_{\mathcal{D}}\int \tilde{g} r_n^* \, dx \, dz. \tag{5.5}$$

In obtaining (5.4) and (5.5) the results

$$\int_{\mathcal{D}}\int r_j r_{kx} \, dx \, dz = 0, \tag{5.6a}$$

and

$$\int_{\mathcal{D}}\int r_j r_k \, dx \, dz = 0, \tag{5.6b}$$

have been used. The derivation of the free mode orthogonality condition is easily modified to obtain (5.6a). Following the analysis in Appendix B it is clear that

$$\nabla \cdot [r_{jt} \underline{D}_n - r_{nt} \underline{D}_j] = i\beta[\omega_n r_j r_{nx} - \omega_j r_n r_{jx}]. \tag{5.7}$$

By integrating (5.7) over the domain D and applying the divergence theorem, Eq. (5.6a) follows. A similar modification to the derivation of (3.5b) leads to Eq. (5.6b)

Consider the case when the time dependence of the wind stress curl is separable, so that $\tilde{g}(x, z, t) = \hat{g}(t)\bar{g}(x, z)$, say. Suppose for $t < 0$ there is no forcing and the ocean is

at rest. For $t \geq 0$ the forcing is applied. Integrating (5.4) gives

$$a_n(t) = -\frac{\omega_n}{|\gamma_n|\beta} \int_0^t g_n(t')\, dt'.$$

Using (5.5) this can be rewritten as

$$a_n(t) = -\frac{\omega_n c_n}{\beta} \int_0^t \hat{g}(t') \exp(i\omega_n t')\, dt', \tag{5.8a}$$

where

$$c_n = \int_{\mathcal{D}}\int \bar{g}\hat{\phi}_n \exp(-i\gamma_n x)\, dx\, dz, \tag{5.8b}$$

and $\hat{\phi}_n$ is defined in Appendix B. Define

$$G_n(t) = \int_0^t \hat{g}(t') \exp(i\omega_n t')\, dt',$$

so that finally

$$p(x, y, z, t) = -2\beta^{-1} \cos(ly) \sum_{n=1}^{\infty} \omega_n \hat{\phi}_n \mathcal{R}\{c_n G_n \exp[i(\gamma_n x - \omega_n t)]\}, \tag{5.9}$$

where $\mathcal{R}$ denotes the real part. The contribution from each mode to the total solution will be assessed by calculating the volume integral of the energy density for that mode:

$$\bar{E}_j = \frac{1}{2} \int_{z=0}^{1} \int_{y=0}^{\lambda_y} \int_{x=0}^{1} \left\{ p_{jx}^2 + p_{jy}^2 + \frac{\sigma^2}{N^2} p_{jz}^2 \right\} dx\, dy\, dz, \tag{5.10}$$

where λ_y is the dimensionless wavelength $2\pi l^{-1}$ and p_j is the pressure field associated with the j^{th} mode. From (5.9) it can be seen that

$$p_j = Q_j \cos(ly)\, \hat{\phi}_j(x, z) \cos(\xi_j),$$

where

$$Q_j = -2\beta^{-1} \omega_j |c_j|\, |G_j|, \qquad \xi_j = \gamma_j x - \omega_j t + \theta_j(t) + \vartheta_j,$$

and

$$c_j = |c_j| \exp(i\vartheta_j), \qquad G_j = |G_j| \exp[i\theta_j(t)].$$

Evaluating (5.10), using (3.3b), gives

$$\bar{E}_j = \frac{1}{4} \lambda_y Q_j^2 \int_{x=0}^{1} \int_{z=0}^{1} \left\{ \hat{\phi}_{jx}^2 + \hat{\phi}_j^2 (l^2 + \lambda_j^2) + \frac{\sigma^2}{N^2} \hat{\phi}_{jz}^2 \right\} \cos^2(\xi_j)\, dx\, dz. \tag{5.11}$$

Equation (5.11) can be simplified to

$$\bar{E}_j = \frac{\lambda_j}{4|\gamma_j|} |c_j|^2 |G_j|^2, \tag{5.12}$$

upon integrating by parts and applying (3.3), (B8) and (B9).

As an example, of this general theory, consider the forced response generated by the dimensionless zonal wind stress (τ is nondimensionalized with τ_0 a typical wind stress magnitude)

$$\tau = \begin{cases} \sin(\mu x)\sin(ly)\,H(b-x)\,H(x-a), & 0 \le t \le T \\ 0, & t > T. \end{cases}$$

In $0 \le t \le T$ the wind stress curl is given by

$$\underline{k}.\mathrm{curl}\underline{\tau} = -l\sin(\mu x)\cos(ly)\,H(b-x)\,H(x-a).$$

Following Gill and Clarke (1974) the wind stress curl is assumed to act as a body force over the mixed layer, in which case (see (5.1))

$$\tilde{g}(x,z,t) = \begin{cases} \dfrac{-l\tau_0}{\rho_* f^2 \delta(x) HL}\sin(\mu x)\,H(T-t)\,H(b-x)\,H(x-a), & z_m \le z \le 1 \\ 0, & \text{otherwise,} \end{cases}$$

where $\delta(x)$ is the depth of the mixed layer (i.e., $\delta = 1 - z_m$). The objective is to determine the values of m and n corresponding to the largest values of $\bar{E}_{m,n}$ (the integrated energy density associated with the non-separable eigenfunction $\phi_{m,n}$). The numerical model is limited to $1 \le m \le 10$. To investigate $\bar{E}_{m,n}$ for larger values of m an analytical solution of (3.3) is used. If h, the mixed layer depth, is constant and N_0, the buoyancy frequency below the mixed layer, is also constant then

$$\phi_{m,n} = \begin{cases} \sin(m\pi x) & 1-h \le z \le 1 \\ \sin(m\pi x)\dfrac{\cos(\alpha_n z)}{\cos[\alpha_n(1-h)]} & 0 \le z \le 1-h, \end{cases}$$

where α_n satisfies the transcendental equation

$$\tan[\alpha_n(1-h)] = -\alpha_n h.$$

A typical mixed layer depth satisfies $h \ll 1$ so that to a good approximation $\alpha_n \approx n\pi$ and $\lambda_{m,n}$ is given by (4.2b). It is now straightforward to work out analytical approximations to γ_j, M_j (see Appendix B), $|c_j|$ and $|G_j|$:

$$\gamma_j^2 = \lambda_j + l^2,$$

$$M_j = \tfrac{1}{2}, \qquad \forall\ m \text{ and } n,$$

$$|c_j|^2 \approx \frac{l^2\tau_*^2(M_j|\gamma_j|)^{-1/2}}{16H^2L^2f^4\rho_*^2}\left\{\left[\int_a^b \sum_{k=1}^{4}(-1)^{k-1}\frac{\sin(r_k x)}{r_k}\right]^2 + \left[\int_a^b \sum_{k=1}^{4}(-1)^{k-1}\frac{\cos(r_k x)}{r_k}\right]^2\right\},$$

where

$$r_1 = m\pi + \mu + \gamma_j, \qquad r_2 = m\pi - \mu + \gamma_j,$$
$$r_3 = -m\pi - \mu + \gamma_j, \qquad r_4 = -m\pi + \mu + \gamma_j,$$

and

$$|G_j|^2 = \frac{4\gamma_j^2}{\beta^2}\left[\sin^2\left(\frac{\beta T}{2\gamma_j}\right) + \left\{1 - \cos\left(\frac{\beta T}{2\gamma_j}\right)\right\}^2\right].$$

Substituting these expressions into (5.12) gives an analytical estimation of the energy density $\overline{E_j}$ associated with each mode. Note that the results of the previous section indicate that for large m (and hence small S) this solution will be a good approximation even when $h = h(x)$. The parameters which determine the form of the free modes are chosen to be the same as case (b) except that $N_0^{-2} = 3.9 \times 10^{-4}$ whereas $N = N(z)$ in case (b). Choosing this value for N_0 gives eigenvalues which are very similar to those found numerically for case (b). Results are presented for the first baroclinic mode and three different wind stress curl forcing fields:

(i) $a = 0.0, b = 1.0, \mu = 52\pi$ and $T = 235.0$ (equivalent to 30.7 days), i.e. cells of wind stress curl across the full width of the channel.

(ii) $a = 50/52, b = 51/52, \mu = 52\pi$ and $T = 235.0$, i.e. a single cell of wind stress curl close to the eastern boundary.

(iii) $a = 8/10, b = 9/10, \mu = 10\pi$ and $T = 235.0$, i.e. as case (ii) except the cell has a larger horizontal extent.

Figure 9 shows plots of $\overline{E}_{m,1}$ versus m for the three different wind stress curls. In case (i) only modes with $m \leq 3$ contain significant energy densities. In case (ii) modes with small m have the largest values of $\overline{E_j}$ but modes with quite large values of m still contain important amounts of energy. Case (iii) is like case (ii) except the energy maximum does not occur for small m but for $m \approx 120$. Consider now the response to each of these wind stress curls applied to the ocean described in case (a) of Section 4. Remember that the free modes for case (a) are distorted by $h = h(x)$ if $m \leq 14$. The response to (i) would be entirely distorted by the presence of the variable depth mixed layer. Energetic modes generated by the single cell wind stress curl (ii) will be distorted by $h = h(x)$ but much of the energy will go into undistorted modes. Case (iii) can be expected to generate a Rossby wave field which is unaffected by horizontal variations in stratification.

Finally, Table 3 presents the eigenvalues and integrated energy density (5.12) for mixed layer depth profiles (a) and (b) in Section 4 using wind stress curl (*i*). Once again the notation of Section 4 is adopted (i.e., $\phi_{i,j}$ is the nonseparable eigenfunction which has i half wavelengths in the x-direction and j half wavelengths in the z-direction). The values of l and μ are assigned to give a wavelength of 500 km in the meridional direction and 270 km in the zonal direction. Also $\tau_0 = 0.1N\ \mathrm{m}^{-2}$, $\rho_* = 1028\ \mathrm{kg\ m}^{-3}$ and $T = 235.0$. The channel is 7000 km wide and 3 km deep (as in Figs. 3

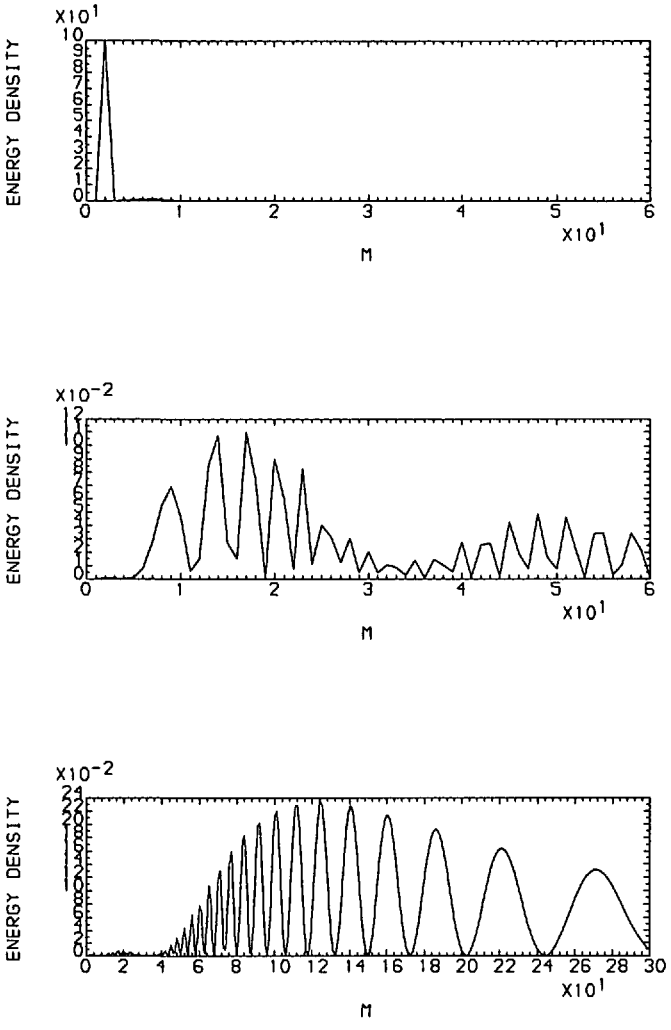

Figure 9. (a) Plot of energy density $\overline{E}_{m,1}$ for wind stress curl (*i*). (b) Plot of energy density $\overline{E}_{m,1}$ for wind stress curl (*ii*). (c) Plot of energy density $\overline{E}_{m,1}$ for wind stress curl (*iii*). Note that m extends to 300 here.

and 4). In Table 3 the energy in each mode, $\overline{E}_{i,j}$, is expressed as a percentage of the total amount of energy contained in all the modes resolved by the model.

From Table 3 it is clear that for both stratifications, almost all the energy is contained in the first baroclinic-type mode with $i \leq 3$. Therefore, the numerical results are in good agreement with the analytical approximations which led to Figure 9(a). However for stratifications (a) and (b) the distribution of energy between the modes differs with respect to the index i. For a constant mixed layer depth $i = 1, 2$ dominate the response, whereas in the Lamb profile $i = 1, 3$ play the major role. Experiments using the analytical results described above indicate that the barotropic and higher

Table 3. Eigenvalues $\lambda_{i,j}$ and energy densities, $\overline{E}_{i,j}$ for mixed layer depth profiles (a) and (b) from Section 3. Wind stress curl (i) is used.

i	j	$\lambda_{i,j}$ Case (a)	$\lambda_{i,j}$ Case (b)	$\overline{E}_{i,j}$ Case (a)	$\overline{E}_{i,j}$ Case (b)
1	0	9.8512	9.8512	2.4×10^{-4}	1.1×10^{-4}
2	0	39.185	39.185	1.8×10^{-4}	8.3×10^{-5}
3	0	87.346	87.346	1.2×10^{-3}	5.8×10^{-4}
4	0	153.26	153.26	4.4×10^{-3}	2.0×10^{-3}
5	0	235.45	235.45	3.5×10^{-3}	1.6×10^{-3}
6	0	332.08	332.08	1.4×10^{-2}	6.6×10^{-3}
1	1	1.907×10^{4}	2.037×10^{4}	44.1	28.9
2	1	1.960×10^{4}	2.040×10^{4}	7.9	55.5
3	1	1.993×10^{4}	2.045×10^{4}	27.2	9.8
4	1	2.021×10^{4}	2.051×10^{4}	11.8	2.4
5	1	2.041×10^{4}	2.060×10^{4}	5.2	3.1
6	1	2.063×10^{4}	2.069×10^{4}	3.8	0.3
1	2	8.729×10^{4}	9.114×10^{4}	1.9×10^{-4}	2.7×10^{-6}
2	2	8.846×10^{4}	9.117×10^{4}	4.8×10^{-4}	8.8×10^{-7}
3	2	8.890×10^{4}	9.122×10^{4}	1.5×10^{-4}	3.8×10^{-5}
4	2	8.933×10^{4}	9.129×10^{4}	1.2×10^{-4}	1.5×10^{-5}
5	2	9.001×10^{4}	9.137×10^{4}	1.0×10^{-3}	4.4×10^{-4}
6	2	9.002×10^{4}	9.146×10^{4}	4.5×10^{-4}	2.4×10^{-3}
1	3	2.1151×10^{5}	2.1643×10^{5}	3.0×10^{-5}	4.8×10^{-9}
2	3	2.1286×10^{5}	2.1646×10^{5}	4.7×10^{-5}	1.1×10^{-7}
3	3	2.1330×10^{5}	2.1651×10^{5}	1.0×10^{-4}	3.2×10^{-8}
4	3	2.1374×10^{5}	2.1657×10^{5}	1.2×10^{-4}	4.0×10^{-7}
5	3	2.1474×10^{5}	2.1666×10^{5}	1.3×10^{-4}	4.3×10^{-8}
6	3	2.1475×10^{5}	2.1675×10^{5}	4.0×10^{-5}	2.7×10^{-7}

baroclinic modes will contain a similar amount of total energy but the modes with most energy are associated with $\phi_{m,n}$ where m is very large. These large values of m often imply unrealistically short horizontal wavelengths.

6. Discussion

In Section 2 the propagation of free Rossby waves in an unbounded continuously stratified ocean with a mixed layer depth, h, which varies zonally is considered analytically. The analysis is restricted to the case in which horizontal variations of h are large compared to a typical horizontal wavelength for the Rossby wave. it is shown that realistic changes in h can produce amplitude modulations of the waves, the largest amplitudes occurring where h is smallest.

In Sections 3 and 4 it is shown how Rossby basin modes can be numerically determined when the buoyancy frequency varies both zonally and with depth. Using the orthogonality properties satisfied by the basin modes, a general theory is presented

in Section 5 for calculating the response generated by a body force acting within the mixed layer.

When a wind stress curl is applied for a finite duration as a body force in the mixed layer, a first baroclinic mode-type response is obtained. Kraus and Wuebber (1982) and Emery and Magaard (1976) have shown that the first baroclinic mode dominates the Rossby wave field in the North Atlantic and North Pacific respectively. When $N = N(x, z)$ (associated with a prescribed climatological mixed layer depth profile at 35N in the Atlantic determined by Lamb, 1984) the eigenfunctions are not separable, but still exhibit the gross features of the separable eigenfunctions associated with $N = N(z)$. It is demonstrated that for certain wind stress curl forcing fields and $N = N(x, z)$, the amplitude of the wave response is concentrated in the region where the mixed layer depth is greatest. The same forcing applied to a constant mixed layer depth (taken to be the zonally averaged Lamb-profile) generates a response which is uniformly distributed over the channel. In the particular case studied numerically here, the two most energetic modes are $\phi_{1,1}$ and $\phi_{3,1}$ (where $\phi_{i,j}$ denotes the eigenfunction with i half wavelengths in the x-direction and j half wavelengths in the z-direction) when $N = N(x, z)$, whereas for a constant mixed layer depth the response is dominated by $\phi_{1,1}$ and $\phi_{2,1}$.

In this paper only zonal variations of h in the absence of mean flows are considered. It is the subject of work currently in progress to extend the analysis to the case of meridional h variations. The associated meridional pressure gradient is in geostrophic balance with a zonal mean flow.

The results discussed here have important implications for the interaction of mixed layer dynamics and baroclinic Rossby waves. Consider the seasonal time scale response of the mixed layer to surface forcing (e.g. the seasonal cycle of the wind stress, net heat flux etc.). The surface forcing will also generate a baroclinic Rossby wave field. The maximum amplitude of the wave field will be patchy; concentrated into regions of either mixed layer depth maxima or minima depending on whether basin modes or free modes unaffected by lateral boundaries are appropriate. Coupling of the mixed layer dynamics and the wave field will be important in these regions. The coupling will, of course, alter the Rossby wave field. This interaction problem is challenging.

Acknowledgments. This research was supported by the UK Natural Environment Council and the UK Ministry of Defence via grant number GR3 6331A. The support is gratefully acknowledged. The authors would also like to thank an anonymous referee for suggesting the ray theory approach of Section 2.

APPENDIX

A. The governing pressure Eq. (2.1)

The objective of this Appendix is to demonstrate that the Rossby wave equation (2.1) is appropriate for distributions of $N = N(x, z)$ caused by realistic mixed layer depth charges. Note that, unless otherwise stated, all quantities in this Appendix are

dimensional. Darby and Willmott (1990) derived the linearized quasi-geostrophic potential vorticity equation which allows variations of $N(y, z)$ in the meridional direction to occur on the internal Rossby radius length scale. An entirely analogous procedure can be applied to derive the linearized quasi-geostrophic potential vorticity equation which allows variations of $N(x, z)$ in the zonal direction to occur on a length scale of several internal Rossby radii, or less (typically tens of kilometers to a few hundred kilometers in the ocean which is an appropriate length scale for typical mixed layer depth changes). The reader is referred to Darby and Willmott (1990) for details of the derivation.

The ocean domain is located on a mid-latitude β-plane. A local Cartesian coordinate system is chosen with x directed eastward, y northward and z vertically upward from the ocean floor located at $z = 0$. The governing equations for large-scale hydrostatic motions in an incompressible Boussinesq fluid are

$$\frac{Du}{Dt} - fv + \frac{1}{\rho_*} p_x = \frac{\tau_z^{(x)}}{\rho_*}, \tag{A.1}$$

$$\frac{Dv}{Dt} + fu + \frac{1}{\rho_*} p_y = \frac{\tau_z^{(y)}}{\rho_*}, \tag{A.2}$$

$$p_z = -\rho g, \tag{A.3}$$

$$\frac{D\rho}{Dt} = 0, \tag{A.4}$$

$$u_x + v_y + w_z = 0, \tag{A.5}$$

where

$$\frac{D}{Dt} \equiv \frac{\partial}{\partial t} + u\frac{\partial}{\partial x} + v\frac{\partial}{\partial y} + w\frac{\partial}{\partial z}, \tag{A.6}$$

and u, v and w denote the velocity components in the x, y, and z directions respectively, ρ denotes density, p denotes pressure, f is the Coriolis parameter, ρ_* is a constant reference density and $\tau^{(x)}$ and $\tau^{(y)}$ denote the body forces in the x and y directions respectively (arising from wind stress at the sea surface, say).

We write $f = f_0 + \beta y$ where f_0 is the value of the Coriolis parameter at the reference latitude of the β-plane. It is now necessary to introduce non-dimensional variables (denoted by primes)

$$(x, y) = L(x', y'), \quad z = Hz', \quad t = \left(\frac{L}{U_0}\right)t', \quad f = f_0 f', \quad \underline{\tau} = \tau_0 \underline{\tau}', \tag{A.7a}$$

where L and H are typical horizontal and vertical length scales respectively, U_0 is a

typical horizontal velocity and τ_0 is a typical value of the body force. We consider quasi-geostrophic motions for which the Rossby number, $\epsilon = U_0/f_0L \ll 1$ and define

$$\left.\begin{aligned} u &= U_0\epsilon u', \quad v = U_0[V(x,z) + \epsilon v'], \quad w = \left(\frac{HU_0}{L}\right)\epsilon w', \\ \rho &= \rho_0(z) + \left(\frac{\rho_* f_0 U_0 L}{gH}\right)[\bar{\rho}(x,z) + \epsilon\rho'] \\ p &= p_0(z) + (\rho_* f_0 U_0 L)[\bar{p}(x,z) + \epsilon p'] \end{aligned}\right\} \tag{A.7b}$$

where ρ_0 and p_0 denote the equilibrium density and hydrostatic pressure fields respectively. Horizontal variations in the basic state density and pressure fields are denoted by $\bar{\rho}(x, z)$ and $\bar{p}(x, z)$. It is important to note that we do not require $\bar{\rho}$ or $\bar{p}$ to be small. Further, V denotes the basic state horizontal velocity which is in geostrophic balance with $\bar{p}(x, z)$. Quantities u', v', w', ρ' and p' denote nondimensional perturbation fields. Taking typical scales to be $L = 100$ km, $U_0 = 0.1$ ms^{-1}, $f_0 = 10^{-4}$ s^{-1}, $\beta = 1.6 \times 10^{-11}$ m$^{-1}s^{-1}$ gives $\epsilon = 0.01$ and suggests we choose

$$f' = 1 + \beta' y', \tag{A.7c}$$

where

$$\beta' = L^2\beta/U_0,$$

so that $\beta' = 1.6$ (i.e. an order one quantity).

Substituting (A.7) into (A.1) to (A.6) gives an equivalent nondimensional set of equations. Following Darby and Willmott (1990) all perturbation quantities (including the body force vector) are expanded as a power series in terms of the small Rossby number, ϵ. Sverdrup balance exists between βV and the curl of the leading order body force, $\tau^{(x)}$. Leading order v' must include a correction to allow thermal wind balance on a β-plane. We must therefore choose the $O(\epsilon)$ body force to be in Sverdrup balance with this correction (in order to obtain an unforced Rossby wave equation). Equating terms of order 1, ϵ and ϵ^2 leads to a closed system of equations which can be solved for the leading order perturbation pressure field, p, namely

$$\left(\frac{\partial}{\partial t} + V\frac{\partial}{\partial x}\right)\left[\nabla_h^2 p + f_0^2\left(\frac{p_z}{N^2}\right)_z\right] - p_y\left[V_{xx} + f_0^2\left(\frac{V_z}{N^2}\right)_z\right] + \beta p_x = 0. \tag{A.8}$$

It is important to note that the body force required to balance the meridional mean flow does not occur in (A8). This is a similar result to that discussed by Pedlosky (1979, Section 7) for the baroclinic instability of nonzonal mean flow. In (A7), $V(x, z)$ is in thermal wind balance with the horizontal mean density gradients associated with $N(x, z)$. If we now neglect V, as discussed in Section 2, we obtain (2.1). Darby and

Willmott (1990) solve the analogous equation to (A8) which considers a prescribed $N(y, z)$ and includes the associated geostrophic mean zonal flow $U(y, z)$.

B. The free mode orthogonality condition

The analysis of this section closely follows that in Clarke (1977) for coastal trapped wave propagation in a continuously stratified ocean. Define

$$r_n = \phi_n \exp\,[i(\gamma_n x - \omega_n t)], \qquad r_n^* = \phi_n \exp\,[-i(\gamma_n x - \omega_n t)]$$

and define the vector fields

$$\underline{D}_n = (r_{nxt} + \beta r_n)\underline{i} + \sigma^2\left(\frac{r_{nzt}}{N^2}\right)\underline{k}$$

and

$$\underline{D}_n^* = (r_{nxt}^* + \beta r_n^*)\underline{i} + \sigma^2\left(\frac{r_{nzt}^*}{N^2}\right)\underline{k}.$$

Once again, ϕ_n, denotes an eigenfunction satisfying the non-separable problem (3.3). The Rossby wave equation (3.3) can be written as

$$\nabla \cdot \underline{D}_n = l^2 r_{nt}, \tag{B1}$$

or

$$\nabla \cdot \underline{D}_n^* = l^2 r_{nt}^*. \tag{B2}$$

Using (B1) and (B2) it is found that

$$\nabla \cdot (r_{jt}^* \underline{D}_n - r_{nt}\underline{D}_j^*) = i\beta(\omega_j r_n r_{jx}^* + \omega_n r_{nx} r_j^*). \tag{B3}$$

Now integrate (B3) over the rectangular cross-sectional area of the basin and employ the divergence theorem to obtain

$$\int_{\partial\mathcal{D}} (r_{jt}^* \underline{D}_n - r_{nt}\underline{D}_j^*) \cdot \underline{n}\, ds = i\beta \int_{\mathcal{D}}\int (\omega_j r_n r_{jx}^* + \omega_n r_{nx} r_j^*)\, dx\, dz, \tag{B4}$$

where $\mathcal{D}$is the cross-sectional area of the basin, $\partial\mathcal{D}$ is the boundary of $\mathcal{D}$, $\underline{n}$ is an outward unit normal vector to $\partial\mathcal{D}$ and ds is an element of the boundary. The left hand side of (B4) is zero by virtue of (3.3b) and so

$$\int_{\mathcal{D}}\int (\omega_j r_n r_{jx}^* + \omega_n r_{nx} r_j^*)\, dx\, dz = 0. \tag{B5}$$

After integrating by parts and applying (3.3b) again, (B5) can be rewritten as

$$(\omega_j - \omega_n) \int_{\mathcal{D}}\int r_n r_{jx}^*\, dx\, dz = 0, \tag{B6}$$

which is the required result. To normalize the orthogonality condition, choose b_n in (3.4) to be given by

$$b_n = (|\gamma_n| M_n)^{-1/2}, \tag{B7}$$

where

$$M_n = \int_{\mathcal{D}}\int \phi_n^2 \, dx \, dz, \tag{B8}$$

and write

$$\hat{\phi}_n = \frac{\phi_n}{(|\gamma_n| M_n)^{1/2}}. \tag{B9}$$

Condition (3.5a) now follows immediately. The orthogonality condition (3.5a), is now used to derive condition (3.5b). It follows from (3.5a) that

$$\int_{\mathcal{D}}\int \hat{\phi}_n(\hat{\phi}_{mx} - i\gamma_m\hat{\phi}_m) \exp[i(\gamma_n - \gamma_m)x] \, dx \, dz = i\delta_{mn}, \tag{B10}$$

$$\int_{\mathcal{D}}\int \hat{\phi}_m(\hat{\phi}_{nx} + i\gamma_n\hat{\phi}_n) \exp[i(\gamma_n - \gamma_m)x] \, dx \, dz = -i\delta_{mn}. \tag{B11}$$

Note that

$$\int_{x=0}^{1} \hat{\phi}_n\hat{\phi}_{mx} \exp[i(\gamma_n - \gamma_m)x] \, dz = -\int_{x=0}^{1} \hat{\phi}_m\left[\hat{\phi}_{nx} + \frac{\hat{\phi}_n}{i(\gamma_n - \gamma_m)}\right] \exp[i(\gamma_n - \gamma_m)x] \, dx \tag{B12}$$

where (3.3b) has been used. Substituting (B12) into (B10) and adding the resulting equation to (B11) leads to

$$\int_{\mathcal{D}}\int \hat{\phi}_n\hat{\phi}_m \exp[i(\gamma_n - \gamma_m)x]\left[\frac{(\gamma_n - \gamma_m)(\gamma_m - \gamma_n) - 1}{\gamma_n - \gamma_m}\right] dx \, dz = 0. \tag{B13}$$

Condition (3.5b) for the case $n \neq m$ follows from (B13). The case when $n = m$ can be derived directly using (B8) and (B9).

C. Numerical solution for the free modes

Equation (3.3a) is solved in $x - z$ space on an $m \times n$ grid of N points ($N = mn$) which are spaced evenly in the x-direction and unevenly in the z-direction. The grid is generated by mapping a regularly spaced $m \times n$ grid in $x - \eta$ space to $x - z$ space. Substituting second-order finite difference approximations into (3.3a) leads to the algebraic eigenvalue problem.

$$\underline{\underline{A}}\,\underline{\underline{\Phi}} = \underline{\underline{\Phi}}\,\underline{\underline{\Lambda}} \tag{C1}$$

where $\underline{A}$ is a real sparse unsymmetric $N \times N$ matrix, $\underline{\Phi}$ is an $N \times N$ matrix of right eigenvectors and $\underline{\Lambda}$ is a diagonal matrix of the corresponding eigenvalues $\lambda_1, \lambda_2 \ldots \lambda_N$. If the eigenvalues are ordered so that $\lambda_1 < \lambda_2 < \cdots < \lambda_N$ then, for $N(x, z)$ and σ typical of the Atlantic at 35N, the eigenvalues tend to occur in well separated clusters corresponding to the barotropic mode, first baroclinic-type mode etc. Within a cluster the eigenvalues are relatively close (see Table 3). The method of simultaneous iteration, described by Jennings and Stewart (1975), is well suited to the solution of such a problem.

Suppose U is an $N \times s$ matrix containing the latest eigenvector estimates. In order to find the smallest eigenvalues the algebraic system of linear equations

$$\underline{A}\,\underline{V} = \underline{U} \tag{C2}$$

must be solved for $\underline{V}$ (an $N \times s$ matrix) at each major iteration of the simultaneous iteration process. Stones's strongly implicit scheme is used to solve (C2). The method is designed to give efficient solution of (C2) where $\underline{A}$ arises from the conventional finite difference representation of a second-order elliptic partial differential equation. A clear description of the method is given by Smith (1985).

REFERENCES

Anderson, D. L. T. and A. E. Gill. 1975. Spin-up of a stratified ocean with application to upwelling. Deep-sea Res., *22*, 583–596.

Anderson, D. L. T. and P. D. Killworth. 1977. Spin-up of a stratified ocean with topography. Deep-sea Res., *24*, 709–732.

Bryan, K. and P. Ripa. 1978. The vertical structure of North Pacific temperature anomalies. J. Geophys. Res., *83*, 2419–2429.

Clarke, A. J. 1977. Observational evidence for wind-forced coastal trapped long waves. J. Phys. Oceanogr., *7*, 231–247.

Darby, M. S. and A. J. Willmott. 1990. On Rossby wave propagation in a meridionally stratified channel. Pure and Applied Geophysics special issue on Ocean Hydraulics. (in press).

Emery, W. J., W. G. Lee and L. Magaard. 1984. Geographic and seasonal distributions of Brunt-Väisälä frequencies and Rossby radii in the North Pacific and North Atlantic. J. Phys. Oceanogr., *14*, 294–317.

Emery, W. J. and L. Magaard. 1976. Baroclinic Rossby waves as inferred from temperature fluctuations in the eastern Pacific. J. Mar. Res., *34*, 365–385.

Gill, A. E. and A. J. Clarke. 1974. Wind-induced upwelling, coastal currents and sea-level changes. Deep-Sea Res., *18*, 685–721.

Jennings, A. and W. J. Stewart. 1975. Simultaneous iteration for partial eigensolution of real matrices. J. Inst. Math. Appl., *15*, 351–367.

Killworth, P. D. 1979. On the propagation of stable baroclinic Rossby waves through a mean shear flow. Deep-Sea Res., *26*, 997–1031.

Kraus, W. and C. Wuebber. 1982. Response of the North Atlantic to annual wind variations along the coast. Deep-Sea Res., *29*, 851–865.

Lamb, P. J. 1984. On the mixed layer climatology of the north and tropical Atlantic. Tellus, *36*, 239–305.

LeBlond, P. H. and L. A. Mysak. 1978. Waves in the Ocean, Elsevier, NY, 602 pp.

Müller, P., R. W. Garwood and J. P. Garner. 1984. Effect of vertical advection on the dynamics of oceanic surface mixed layer. Annales Geophysicae, *2,* 387–398.

Mysak, L. A. 1978. Wave propagation in random media with oceanic applications. Reviews of Geophysics and Space Physics, *16,* 233–261.

Mysak, L. A. and M. S. Howe. 1976. A kinetic theory for internal waves in a randomly stratified fluid. Dyn. of Atmosph. Oceans, 3–31.

Pedlosky, J. 1979. Geophysical Fluid Dynamics. Springer Verlag, NY, 624 pp.

Smith, G. D. 1985. Numerical Solution of Partial Differential Equations: Finite Difference Methods, Oxford University Press.

Stevenson, J. W. 1983. The seasonal variation of the surface mixed-layer response to the vertical motions of linear Rossby waves. J. Phys. Oceanogr., *13,* 1255–1268.

Willmott, A. J. and J. A. Johnson. 1979. The effects of horizontal momentum exchange on the spin-up of a stratified ocean. Deep-Sea Res., *26,* 1247–1266.

Willmott, A. J. and L. A. Mysak. 1980. Atmospherically forced eddies in the Northeast Pacific. J. Phys. Oceanogr., *10,* 1769–1791.

Whitham, G. B. 1974. Linear and nonlinear waves. Wiley, NY, 636 pp.

Received: *27 October, 1988;* revised: *29 March, 1990.*